"REACTIVE IMAGING" OF NANOSTRUCTURED MATERIALS

Keith J. Stevenson and Joseph T. Hupp
Department of Chemistry, Northwestern University, Evanston, IL 60208

Newly developed methodologies are presented in which differential chemical and electrochemical reactivity can be temporally and spatially imaged and subsequently correlated with structural characteristics of nanostructured materials: an approach that we term "reactive imaging". By utilizing a combination of electrochemical methods and integrated optical and atomic force microscopies, a variety of experimental schemes can be proposed. Several preliminary examples are presented to illustrate the resolving power of these coupled techniques. In particular, the dissolution or "molecular corrosion" of luminescent thin films of the "molecular square" compound, $[Re(CO)_3(Cl)(\mu\text{-pyrazine})]_4$ in aqueous nitrobenzene solutions is examined. Simultaneous acquisition of luminescence and topographical data allows for estimation of the crystal dissolution rate. Additionally, the electrochromic stability of a conductive organic polymer (polyaniline) and a redox-active metal oxide (WO_3) are examined by employing two different reactive imaging schemes to correlate charge/ion transfer reactivity with film morphology.

INTRODUCTION

Many technological and industrial processes result from electrochemical reactions (i.e., oxidation and reduction) occurring at solid/liquid interfaces. The refining and deposition of materials (1), the recycling and synthesis of chemicals (2), and the conversion of chemical and photonic energy to electrical energy (3) are examples of processes that occur at these interfaces. In general, the rates of these electrochemical reactions depend on either or both of two component processes: the rate of mass transport of reactants (i.e., ions and molecules) from the bulk solution to a region near a charged surface, and the rate of charge transfer. The rate of an electrochemical process is directly influenced by the applied electric potential and interfacial structure. Due to the complex nature of the solid/liquid interface, energetically nonuniform regions can exist, resulting in spatially heterogeneous electrochemical activity. Thus, a detailed understanding of the intricate relationships between mass transport (e.g., diffusion and convection), surface reactivity (e.g., catalysis, corrosion, and passivation) and interfacial structure (e.g., composition, crystalline orientation, and heterogeneity) is essential for exercising efficient and productive control over electrochemical processes.

A variety of approaches have been reported for mapping spatial variations in electrochemical activity, including high resolution scanning probe microscopies such as

AFM, STM, SECM and NSOM (4). While these techniques provide high resolution surface maps, they are generally poorly suited for mass transfer investigations in that the imaging process is typically too slow (~1-30 min) and the probe itself often perturbs the diffusion profile of the electrochemical event. For this reason, several researchers have employed luminescence (5) and fluorescence (6) microscopies to characterize the spatial distribution of electrochemical activity on a surface. These methodologies are capable of following mass transfer and ion/charge transfer reactions on much faster time scales (generally >200 ns) by collecting light from a luminescence producing reaction or probe with an imaging detector (CCD). Additionally, chemical information is obtained by choosing an appropriate spectroscopic (typically, chemiluminescent) probe molecule. However, in order to obtain a more quantitative understanding of the electrochemical process, these methods are generally coupled with an ex-situ measurement of the surface structure. To date, very few reports have described simultaneous optical and topographical imaging of heterogeneous electrochemical activity with a single integrated instrument (7).

In our laboratory, we are particularly interested in developing new strategies for investigation of ion/charge transfer reactivity at redox-active metal oxides, and molecular and ionic mass transport in mesoporous molecular materials. Due to the diversity of chemistry and materials under study, we have decided to take a "broad-based" approach by utilizing a single integrated instrument, consisting of a free-standing AFM (Digital Instruments Bioscope) mounted on the stage of an inverted optical microscope (Nikon Eclipse TE300). This allows for greater experimental flexibility in that on-axis atomic force and optical images can be acquired simultaneously (or subsequently) on a sample of interest. The only limitation is that the sample must be somewhat transparent to the wavelength of light utilized for optical microscopy. Herein, we describe a versatile approach for the study of solid/liquid interfaces in which differential chemical and electrochemical reactivity can be spatially and temporally imaged and correlated with high resolution structural maps. We propose several imaging strategies and provide some illustrative examples to demonstrate the resolving power of this integrated methodology.

EXPERIMENTAL

Integrated Atomic Force and Optical Microscopies

Figure 1 illustrates the setup and instrumental configuration for integration of the optical and atomic force microscopies. Atomic force microscopy was performed by using a Digital Instruments Bioscope AFM with a Nanoscope IIIa controller. All measurements were obtained in tapping mode with single etched silicon (TESP) Nanoprobe SPM tips (cantilever length 125 μm and resonance frequency 307-367 Hz, Digital Instruments). Photo-induced luminescence microscopy studies (probe molecule studies and backlighting studies; see below) were performed by using a Nikon TE300 inverted microscope in an epi-fluorescence configuration. A 100 W mercury lamp was used together with a Nikon Plan Fluor (60 X /NA = 0.70) objective, a 365 nm band pass excitation filter, a 400 nm dichroic mirror and a 450 $\pm$ 65 nm band pass emission filter.

Imaging experiments with the luminescent films (as opposed to dissolved probe molecules) were conducted with the aforementioned objective, but a 485 nm band pass excitation filter, a 510 dichroic mirror and a 535 $\pm$ 35 band pass emission filter were used. Digital images were acquired with an intensified, precooled (-25 °C) CCD camera (PentaMax, Princeton Instruments, Inc). Image analysis and processing (flatfielding and background subtraction) were conducted using software supplied by Princeton Instruments (WinView/32) and Scion Corp. (Scion Image, version Beta 3b).

Materials and Electrochemical Apparatus

The synthesis of $([Re(CO)_3(Cl)(\mu\text{-pyrazine})]_4$ has been reported elsewhere (8). Thin films of luminescent "molecular squares" (see molecular structure and space-filled representation of array structure, below) were deposited by solvent evaporation from a chloroform/acetonitrile (~1/1 ratio) solution onto precleaned microscope slides (Fisher). Electrochromic polyaniline and tungsten trioxide thin films were prepared by electrochemical methods as described in the literature (9,10). All chemicals and solvents were obtained from Aldrich. Aqueous solutions were prepared by using water obtained from a water purification system (Barnstead Millipore) fed by an in-house distilled water line.

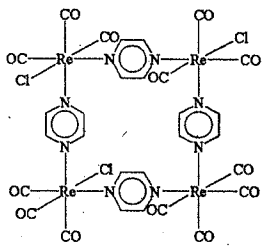

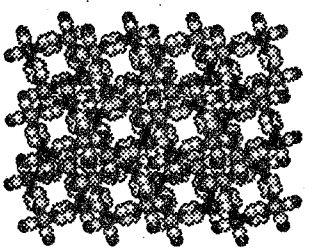

Voltammetric measurements were made by using a BAS model CV-27 potentiostat and a Houston Instruments XY recorder. A homebuilt, one-compartment, three electrode Kel-F cell was used for simultaneous optical and electrochemical measurements. Electrochromic films grown on transparent, conductive indium-tin-oxide (ITO) substrates (Delta Technologies, LTD., 10 ohm/square) were used as working electrodes and Pt wire and Ag/AgCl (BAS, 3 M NaCl) were employed as the counter and reference electrodes, respectively.

RESULTS AND DISCUSSION

By employing a combination of electrochemical methods and integrated optical and atomic force microscopies, a variety of imaging strategies can be proposed, as illustrated in Figure 2. We have termed this versatile approach "reactive imaging" since our focus is

on temporally and spatially mapping differential chemical and electrochemical reactivity of microstructured and nanostructured thin-film materials. In scheme I (AFM monitoring), the strategy is to follow structural changes induced by chemical or electrochemical means on non-luminescent, non-transparent thin films via atomic force microscopy. In scheme II (luminescence monitoring), the strategy is to follow luminescence intensity changes of thin films using optical microscopy. Depending upon luminescence characteristics of the thin film several different experiments can be envisaged. For instance, a chemical sensing event can be monitored as the film luminescence is quenched due to selective chemical binding of an introduced analyte. In scheme III (fluorescence monitoring), the strategy is to utilize solution-phase fluorescent dye molecules as local reporters on electrochemically-induced ion or pH changes. In scheme IV (inner-filter-absorbance/fluorescence monitoring), the strategy is to follow changes in film absorbance by utilizing solution fluorescence as a means for providing image contrast by a process of "backlighting". Below, are some illustrative experimental examples of these reactive imaging strategies.

Luminescence Imaging of Molecular Corrosion

In our laboratory, we have been interested in the study of luminescent transition-metal containing cyclophanes ("molecular squares") as mesoporous thin-film sensing elements. Several studies indicate that these compounds may prove useful as molecular-sieving or possibly, light-responsive, volatile organic chemical sensing devices (11). We have employed the reactive imaging strategies to investigate the stability of these materials in aqueous environments. Figure 3 shows a luminescence imaging experiment that is based on schemes I and II. Figure 3a shows an AFM image of a luminescent thin film comprising a "molecular square" compound, $[Re(CO)_3(Cl)(\mu\text{-pyrazine})]_4$. One can observe fairly large crystallites or "strands" (~5 μm in length) imbedded in an apparently amorphous thin film. These films are generally insoluble in water; however, introduction of a rather high concentration (~ 0.02 M) of a nonaqueous analyte or co-solvent such as nitrobenzene (NB) causes the films to dissolve. Figure 3b shows the result of a luminescence imaging experiment involving exposure of a film to an aqueous NB solution. Within a period of 8 minutes (a time frame nearly to fast to image with in situ AFM) nearly all of the crystallites are observed to corrode or dissolve. By obtaining luminescence images over this time frame and subsequently correlating with AFM measurements of crystallite size, Figure 3c, a calibration of luminescence intensity with crystal volume can be achieved. Taking into account the known crystal density (d = 1.67 g/cm^3, determined by XRD), analysis of the calibrated luminescence images allowed for estimation of the "molecular corrosion" or crystal dissolution rate, Figure 3d. Note that the crystal dissolution rate is initially slow, but then apparently increases as the reaction progresses.

Fluorescent Imaging of an Electrochemically-generated pH Gradient

We are also particularly interested in elucidation of fundamental factors controlling ion/charge transfer reactivity at inorganic semiconducting thin films. We have observed that electron addition to wide bandgap, nanocrystalline, semiconductors induces

interfacial ion transfer (12). In aqueous environments, the ion taken up is generally H^+. We reasoned that in unbuffered or poorly buffered solutions, interfacial ion transfer reactions involving nanocrystalline metal oxides would induce significant transient local changes in ion concentration. As a model system, we chose to investigate the behavior of an organic semiconductor, polyaniline. The electroreduction of polyaniline is accompanied by charge-compensating proton uptake, leading to a pH jump in the immediate vicinity of the electrode. By employing a pH sensitive dye (7-hydroxycoumarin, $pK_a \sim 7$) we hoped to image localized pH changes. Figure 4 shows a fluorescence imaging experiment that is based on reactive imaging scheme III. The resulting structure of an electropolymerized polyaniline film on ITO is shown in Figure 4a. Large polymeric "blobs" are observed which show up as "white spots" in the AFM height image. Higher resolution AFM images (1 x 1 μm^2 area) indicate that the film morphology is characterized by close packed, spherical domains of 10 to 60 nm diameter. Figure 4b shows the results of a fluorescence imaging experiment as the polyaniline film is switched from an oxidized, conductive state (+0.8 V vs Ag/AgCl) to a reduced, insulating state (-0.8 V). Note that the "white spots" pictured in Fig 4a show up as darker regions in Fig. 4b, due to variation in the optical density of the polyaniline film. Although, we were unable to image the direct uptake of protons by the polyaniline film, we did observe the creation of localized pH gradients within the film due to the electrochemical reduction of water and oxygen, eqs. 1 and 2.

$$2H_2O + 2e^- \rightleftharpoons 2OH^- + H_2 \qquad [1]$$

$$O_2 + 2H_2O + 4e^- \rightleftharpoons 4OH^- \qquad [2]$$

Preliminary analysis of the fluorescence imaging experiment suggests that we are effectively imaging localized breakdown of the polyaniline film. Localized electrochemical reduction of water produces hydrogen gas, which in turn, produces voids within the polymeric film. The voids fill with dye-containing solution enriched in hydroxide, such that enrichment leads to dye deprotonation and enhanced fluorescence. We speculate that localized heating by the electrolytic reaction induces convective solvent flow (thermocapillary flow) (13), thereby accounting for an apparent transport of small pockets of hydroxide-enriched solution toward larger voids in the film.

Inner-filter-absorbance/Fluorescent Imaging of Ion Intercalation

We have also become interested in ion transfer reactions/intercalation reactions involving redox-active metal oxides (e.g., MoO_3 and WO_3) capable of functioning as electrochromic and energy-storage materials (3c). Recently, we have described a procedure for preparing patterned metal oxide thin films on transparent conductive substrates (14). We have employed the imaging strategies to investigate the electrochromic stability of patterned WO_3 thin films in aqueous environments. Figure 5

shows an inner-filter absorbance/fluorescence imaging experiment that is based on reactive imaging scheme IV. Figure 5a shows an AFM image of a patterned WO_3 thin film on ITO. Higher resolution AFM images (5 x 5 μm^2 area) indicate that the film possesses an amorphous structure consisting of spherical particles ranging in size from 60 to 180 nm. Figure 5b shows the result of an inner-filter-absorbance/fluorescence experiment for the same film shown in Figure 5a as the electrochemical potential is jumped to a negative value (-0.6 V vs Ag/AgCl). Electrochemical reduction of the WO_3 thin film causes the simultaneous intercalation of charge compensating protons which produces a color change from transparent to blue, eq. 3.

$$WO_3 \text{ (transparent)} + xe^- + xH^+ \rightleftharpoons H_xWO_3 \text{ (blue)} \qquad [3]$$

By utilizing the fluorescence from an illuminated solution-phase dye to provide image contrast, changes in the optical density (film absorbance) due to reaction 3 can be monitored. As demonstrated in Fig. 5 this reactive imaging scheme indicates that differential electrochemical reactivity can be successfully spatially imaged and subsequently correlated with structural features. In addition, if the film extinction coefficient is known, a plot of change in film absorbance with time will provide an approximate measure of proton diffusion. From a preliminary analysis of this experiment, the electrochromic behavior (coloration and bleaching) appears to depend strongly upon film microstructure/nanostructure -- most notably, thermally induced changes in micro-/nanocrystallinity. Specifically, the structural changes directly influence the film-based proton diffusivity and the electrochromic stability. A more detailed account of these effects will be presented elsewhere.

SUMMARY

Newly developed "reactive imaging" methodologies have been presented and several preliminary examples are provided to demonstrate the utility of combining electrochemical methods with integrated atomic force and optical microscopies. With this experimental approach we hope to contribute to the fundamental understanding of the function and performance of nanostructured materials employed as thin film electrochromic and photoluminescent devices and provide an impetus for the development of advanced high-resolution imaging techniques for the study of electrified solid/liquid interfaces.

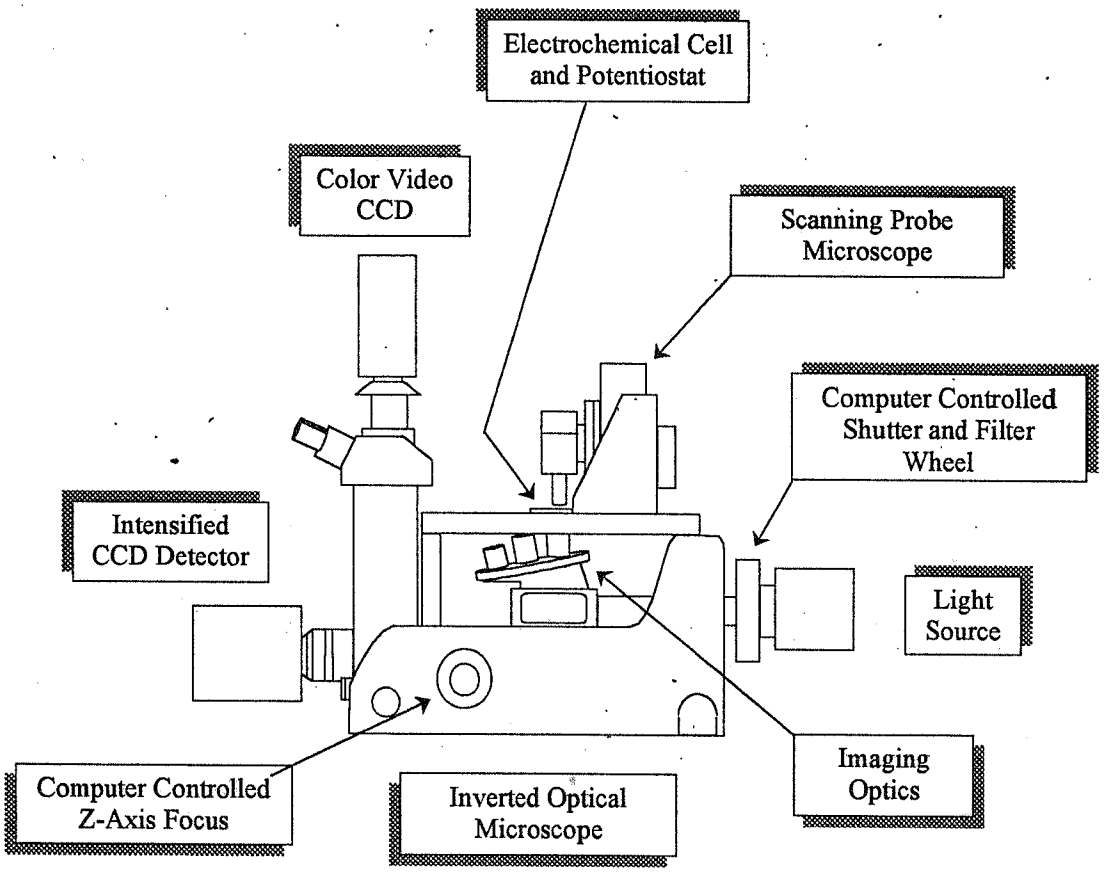

Figure 1. Schematic diagram of integrated optical and atomic force microscopies.

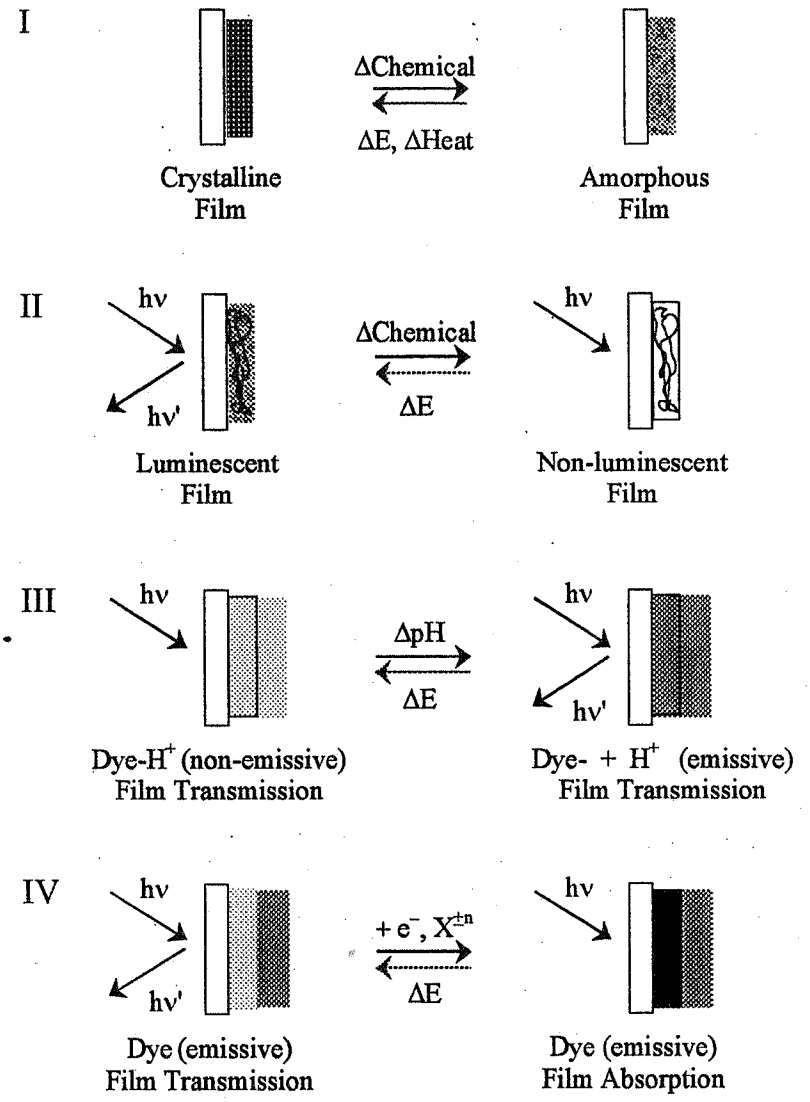

Figure 2. Illustrative representation of a variety of proposed "reactive imaging" schemes for investigation of differential chemical and electrochemical reactivity. Imaging strategies for following induced changes (physical, chemical and electrochemical) in thin films: I) Atomic force monitoring; II) Luminescence monitoring; III) Fluorescence monitoring; IV) Inner-filter-absorbance/fluorescence monitoring.

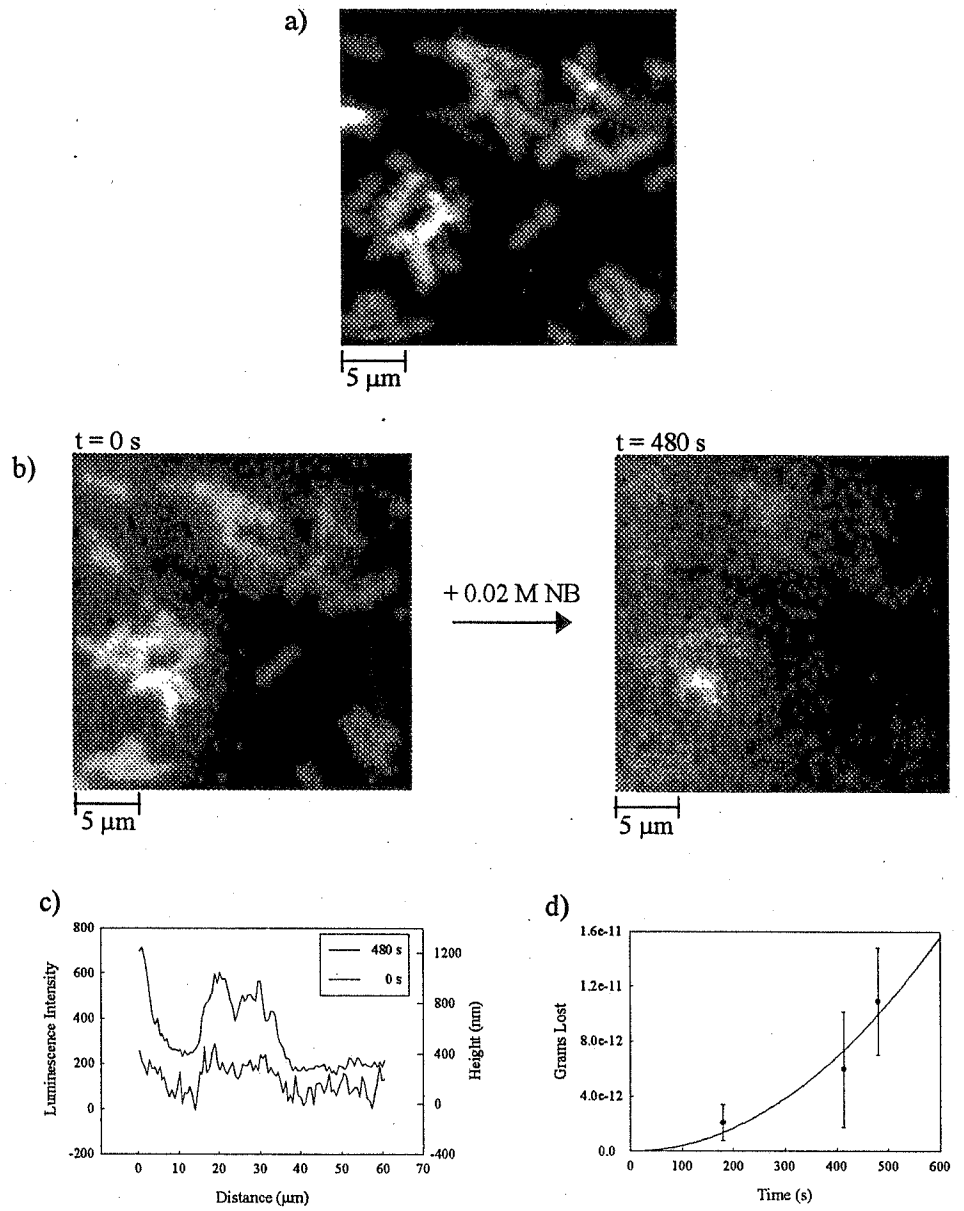

Figure 3. Reactive imaging experiment following a combination of schemes I and II showing "molecular corrosion" of a luminescent thin film comprised of "molecular square" crystallites, $[Re(CO)_3(Cl)(\mu\text{-pyrazine})]_4$. a) AFM image of a luminescent thin film. (b) Luminescence imaging of crystal dissolution following exposure to an aqueous 0.02 M NB solution. c) Cross-sectional plot of luminescence intensity and derived (calibrated) AFM height versus lateral distance. d) Estimation of extent of molecular corrosion of a single cluster of crystallites (total grams lost) versus time.

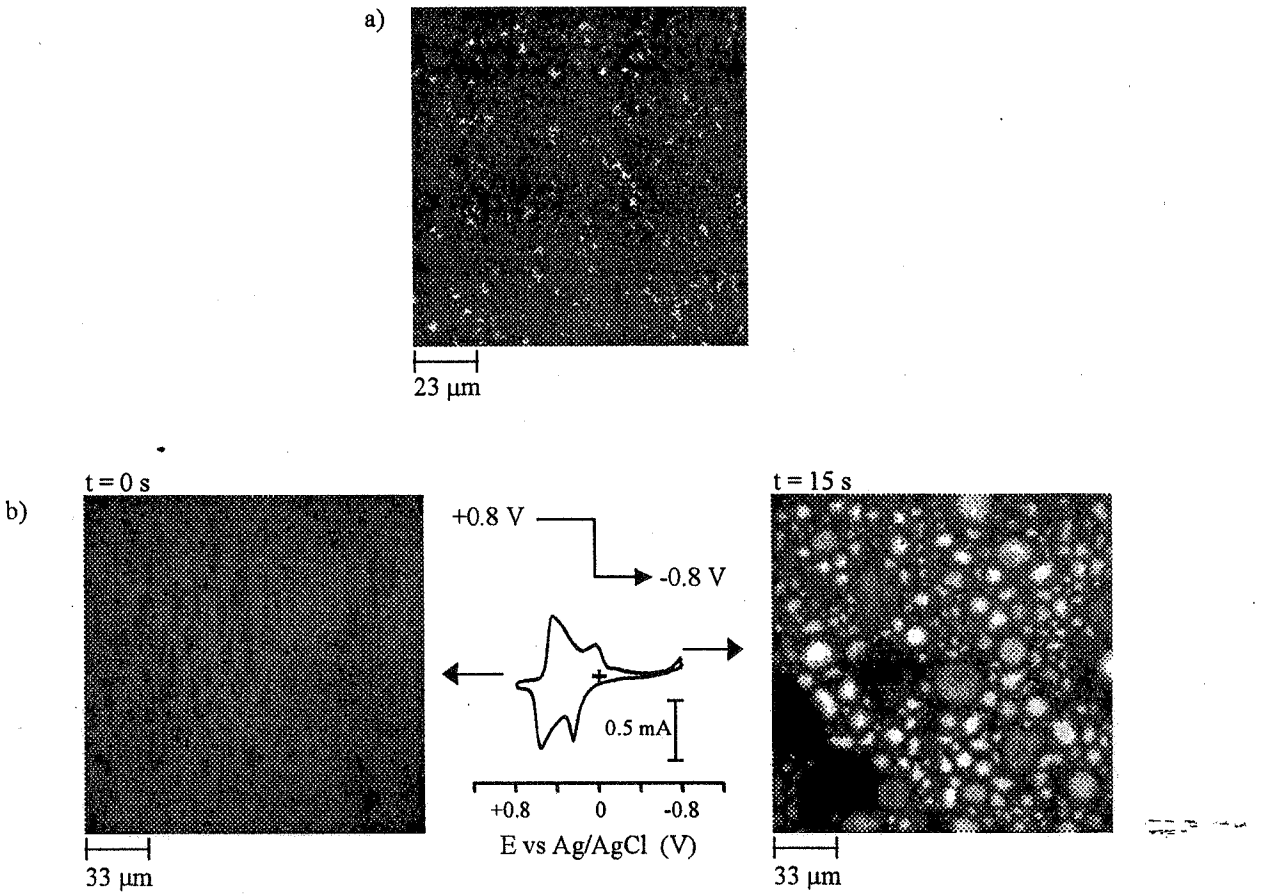

Figure 4. Reactive imaging experiment following scheme III showing localized pH activity due to an electrochemically-induced pH jump at a polyaniline/ITO interface. a) AFM image of electropolymerized polyaniline on an ITO substrate. b) Fluorescent imaging experiment of an electrochemically-induced pH jump at the polyaniline/ITO interface. The fluorescent dye (7-hydroxycoumarin, $pK_a \sim 7$) becomes fluorescent with the production of localized hydroxide due to deprotonation of the dye.

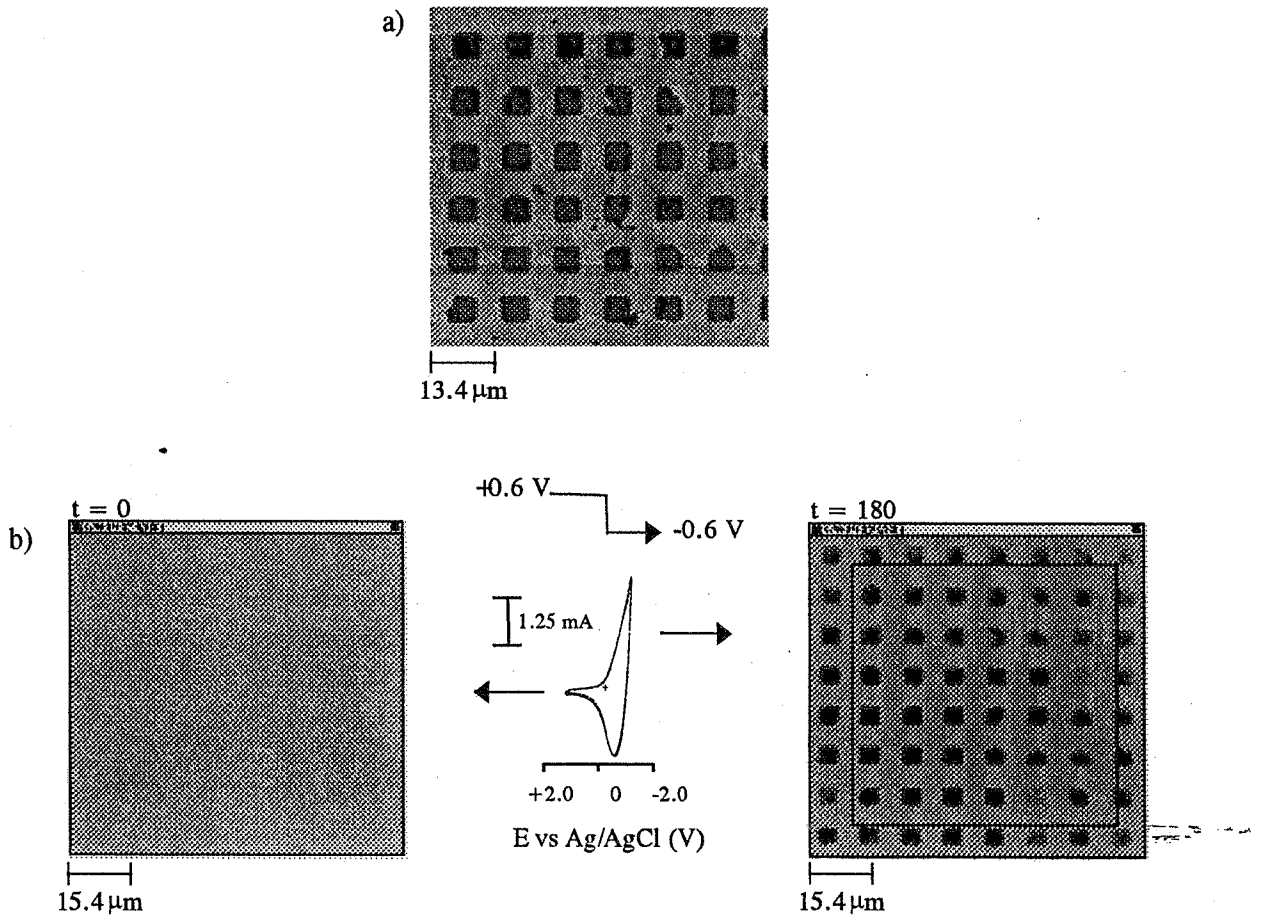

Figure 5. Reactive imaging experiment following scheme IV showing electrocoloration of a patterned WO_3 thin film on ITO. a) AFM image of the patterned WO_3 thin film. b) Inner-filter-absorbance/fluorescence imaging experiment showing the intercalation of protons during reduction of the patterned WO_3 thin film. Black box indicates corresponding area as imaged by AFM above. Note that not all "cells" undergo electrocoloration at the same time.

REFERENCES

1. For example see: (a) D. Kolb, in Advances in Electrochemistry and Electrochemical Engineering, Gericher, H., Tobias, C. W., Editors, Vol. 11, p. 125, Wiley, New York (1978). (b) R. W. Murray, Annu. Rev. Mater. Sci., **14**, 145 (1984).

2. Some reviews include: (a) A. T. Kuhn, Industrial Electrochemical Processes, Elsevier, Amsterdam (1971). (b) T. Shono, Electroorganic Chemistry as a Tool in Organic Synthesis, Springer-Verlag, Berlin (1984). (c) J. O'M. Bockris, Electrochemistry of Cleaner Environments, Plenum Press, New York (1972).

3. For example see: (a) D. Linden, Handbook of Batteries and Fuel Cells, McGraw-Hill, New York (1983). (b). A. Henglein and H. Weller, Photochemical Energy Conversion, J. Norris and D. Meisel, Editors, Elsevier, New York (1989). (c) C. G. Granqvist, Handbook of Inorganic Electrochromic Materials, 1st ed., Elsevier, Amsterdam (1995).

4. For reviews of these techniques, see for instance: (a) Nanoscale Probes of the Solid/Liquid Interface, A. Gewirth, and H. Siegenthaler, Editors, Kluwer Academic Publishers, Boston (1993). (b) Electrochemical Interfaces: Modern Techniques for In-Situ Interface Characterization, H. D. Abruna, Editor, VCH Publishers, New York (1995). (c) A. J. Bard, F.-R. F. Fan, and M. V. Mirkin, in Electroanalytical Chemistry, A. J. Bard, Editor, Vol. 18, p. 244, Marcel Dekker, New York (1994).

5. (a) R. C. Engstrom, C. M. Pharr, M. D. Koppang, J. Electroanal. Chem., **221**, 251 (1987). (b) R. C. Engstrom, K. W. Johnson and S. DesJarlais, Anal. Chem. **59**, 670 (1987). (c) P. Pantano and W. G. Kuhr, Anal. Chem., 65, 2452 (1993). (d) S. E. Rosenwald, N. Dontha and W. G. Kuhr, Anal. Chem., 70, 1133 (1998).

6. (a) R. C. Engstrom, S. Ghaffari and H. Qu, Anal. Chem., **64**, 2525 (1992). (b) S. Fiedler, R. Hagedorn, T. Schnelle, D. Richter, B. Wagner and G. Fuhr, Anal. Chem. **67**, 820 (1995). (c) W. J. Bowyer, J. Xie and R. C. Engstrom, Anal. Chem., **68**, 2005 (1996). (d) J. E. Vitt and R. C. Engstrom, Anal. Chem., **69**, 1070 (1997). (e) K. S. Bronk, K. L. Michael, P. Pantano and D. R. Walt, Anal. Chem., **67**, 2750 (1995). (f) A. A. Panova, P. Pantano and D. R. Walt, Anal. Chem., **69**, 1635 (1997). (g) M. Alodan and W. H. Smyrl, J. Electrochem. Soc., **145**, 1571 (1998). (h) M. Alodan and W. H. Smyrl J. Electrochem. Soc., **144**, L282 (1997). (I) D. S. Chung and R. C. Alkire, J. Electrochem. Soc., **144**, 1529 (1997)

7. P. I. James, L. F. Garfias-Mesias, P. J. Moyer and W. H. Smyrl, J. Electrochem. Soc. **145**, L64 (1998).

8. R. V. Slone and J. T. Hupp, Inorg. Chem., **35**, 4096 (1996).

9. V. Brandl and R. Holze, Ber. Bunsen. Phys. Chem., **101**, 251 (1997).

10. E. A. Meulenkamp, J. Electrochem. Soc., **144**, 1664 (1997).

11. (a) R. V. Slone, K. D. Benkstein, S. Bélanger, J. T. Hupp, I. A. Guzei, and A. L. Rheingold, Coord. Chem. Rev., **171**, 221 (1998). (b) S. Bélanger, J. T. Hupp, C. L. Stern, R. V. Slone, D. F. Watson, and T. M. Carrell, J. Am. Chem. Soc., in press. (c) S. Bélanger, M. H. Keefe, J. Welch and J. T. Hupp, Coord. Chem. Rev., submitted.

12. (a) L. A. Lyon and J. T. Hupp, J. Phys. Chem., **99**, 15718 (1995). (b) B. I. Lemon and J. T. Hupp, J. Phys. Chem., **100**, 14578 (1996). (c) B. I. Lemon and J. T. Hupp, J. Phys. Chem. B., **101**, 2426 (1997).

13. S. A. Guelcher, Y. E. Solomentsev, P. J. Sides, and J. L. Anderson, **145**, 1848 (1998).

14. K. J. Stevenson, G. J. Hurtt and J. T. Hupp, Electrochem. and Solid State Letters, submitted.